

Experimental study of vibration characteristics of FRP cables based on Long-Gauge strain

Qi Xia^a, JiaJia Wu^b, XueWu Zhu^c and Jian Zhang^{*}

Jiangsu Key Laboratory of Engineering Mechanics, School of Civil Engineering, Southeast University, Nanjing, P.R. China

(Received December 25, 2016, Revised March 20, 2017, Accepted June 2, 2017)

Abstract. Steel cables as the most important components are widely used in the certain types of structures such as cable-supported bridges, but the long-span structures may result in an increase in fatigue under high stress and corrosion of steel cables. The traditional steel cable is becoming a more evident hindrance. Fiber Reinforced Polymer (FRP) cables with lightweight, high-strength are widely used in civil engineering, but there is little research in vibrational characteristics of FRP cables, especially on the damping characteristic. This article studied the two methods to evaluate dynamical damping characteristic of basalt FRP(BFRP) and glass FRP(GFRP) cables. First, the vibration tests of the B/G FRP cables with different diameter and different cable force were executed. Second, the cables forces were calculated using dynamic strain, static strain and dynamic acceleration respectively, which were further compared with the measured force. Third, experimental modal damping of each cables was calculated by the half power point method, and was compared with the calculation by Rayleigh damping theory and energy dissipation damping theory. The results indicate that (1) The experimental damping of FRP cables decreases with the increase of cable force, and the trend of experimental damping changes is roughly similar with the theoretical damping. (2) The distribution of modal damping calculated by Rayleigh damping theory is closer to the experimental results, and the damping performance of GFRP cables is better than BFRP cables.

Keywords: cable force; damping ratio; B/GFRP cable; long-gauge strain; vibration test

1. Introduction

Cables, as a significant load carrying structural member, have a widespread application in civil engineering (Irvine and Caughey 1974, Ye *et al.* 2014, Li and Ou 2015). In the operational conditions, traditional steel cable has some limitations such as sag, corrosion, and fatigue. So, the use of lightweight, high-strength materials can overcome the problems and improve structural performance. Fiber Reinforced Polymer (FRP) materials like carbon-FRP, glass-FRP and basalt-FRP have been widely used, because their mechanical and chemical properties are superior to traditional materials in some ways (Nabil 2000, Cheng *et al.* 2006, Wu *et al.* 2009, Upadhyay and Kalyanaraman 2010).

The vibration characteristics of FRP cables have become a key concern in predicting the dynamic stability of long span FRP-cable-stayed bridges. Because the characteristics of FRP cables have the advantage of lightweight and high-strength, which lead to bigger difference in structural dynamic characteristics. One of the primary parameters affecting the susceptibility of the cables during vibration is the cable damping (Fujino 2007, Ye *et al.* 2016, Kim *et al.* 2017). For conventional long cables, whose lower natural

frequency will have a higher risk of resonance between the cables and the deck of bridge, and large dimensions will induce more load effects (Caetano 2007, Wu and Cai 2010).

In order to improve the calculation accuracy and ensure the safety of bridge structure in engineering, a reasonable damping calculation method is needed. At present, there are two general methods: Rayleigh damping theory and energy dissipation damping theory. Yamaguchi and Ito (1997) studied the modal parameters of cable through free vibration response and forced vibration response respectively, and proposed the energy dissipation damping theory to estimate the modal damping ratio. El Kady *et al.* (1999) researched the energy dissipation characteristics of steel cable and CFRP cable, and estimated the energy loss factor of the steel cables are 0.05. Xie *et al.* (2008) compared the difference of damping between steel cable and CFRP cable through energy dissipation damping theory, and indicated that the energy dissipation damping theory is more reasonable for steel cable than CFRP cable. Wang and Wu (2010) used the energy dissipation damping theory to evaluate damping ratio of hybrid basalt and carbon FRP cable with smart dampers. Yang *et al.* (2015) studied on the modal damping ratios of CFRP and BFRP cables through the experiments. In addition, the real ambient measurements are often like that of the lower frequency range of the spectrum and is not so clear due to the type of excitations, sensitivity, and location of the sensors (Ren *et al.* 2005a). Picking the peak is basically a subjective task. Particularly, the identification of cable damping by using PSD (power spectral density) is not always reliable. The vibration response of cable is generally collected by accelerometer

*Corresponding author, Professor
E-mail: jian@seu.edu.cn

^aPh.D.

^bGraduate Student

^cMaster

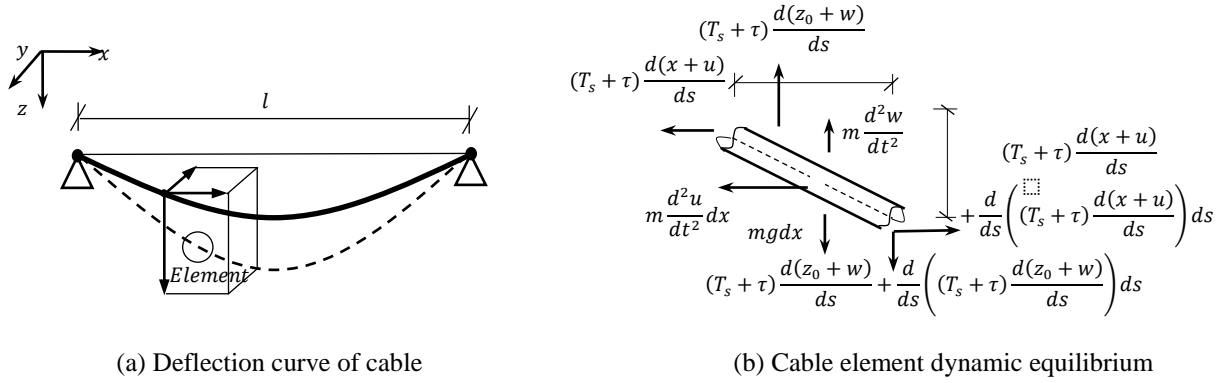


Fig. 1 Vibration model of the horizontal cable

insensitive to the low order response. Thus, when the cable has low natural frequency, the natural frequency estimation is not accurate by acceleration method.

Since the damping mechanism is very complicated, the damping matrix of multiple-degree-of-freedom system generally does not meet the criterions of Rayleigh damping, and the modal damping does not affect each other. When tension of the potential energy has a larger proportion, it is more difficult to get reasonable damping ratio. Besides, the damping calculation is affected by the energy loss factor of different materials. In order to evaluate the GFRP and BFRP damping characteristics, this study use the long-gauge strain sensors to identify the modal parameters of cables, and discuss BFRP and GFRP damping calculation by using the energy dissipative damping theory and the Rayleigh damping theory.

This study is organized as follows: (1) The vibration theory of cable and long gauge strain modal theory briefly introduced. (2) The vibration tests of BFRP and GFRP cables with different diameters were carried out. (3) The modal parameters of the cables have been measured and identified by long-gauge strain sensors and accelerometers. (4) The modal damping calculation has been discussed by using the energy dissipative damping theory and the Rayleigh damping theory and the damping performance of BFRP and GFRP cables were compared.

2. The theory of cable vibration and long-gauge strain

2.1 The theory of cable vibration

String vibration theory (Russell and Lardner 1998) is the rationale of cable tension measurement. The analysis of the cable dynamics shows that the physical model is similar to a beam under the axial tension as shown in Fig. 1, and Fig. 1(b) shows the mechanical equilibrium analysis at any position.

If considering cable's flexural stiffness EI , the free vibration equation of the linear density suspension cable can be established by using dynamics general principle when the damping is not included

$$m \frac{\partial^2 u}{\partial t^2} + EI \frac{\partial^4 u}{\partial x^4} - T \frac{\partial^2 u}{\partial x^2} = 0 \tag{1}$$

where, $u(x, t)$ =crosswise displacement function. m =thelinear density of string. EI =flexural stiffness of cable. T =the tension force. t =the time.

When both cable's boundary conditions of the component can be simplified as hinge, the solution of Eq. (1) is

$$T = 4 \frac{m f_n^2 l^2}{n^2} - \frac{n^2 \pi^2 EI}{l^2} \tag{2}$$

where, l =the effective length of the cable. f_n =the n^{th} natural frequency. n =the vibration order.

When the flexural stiffness EI of cable is very small, such as $\mu = l\sqrt{T/EI} > 80$, it can be ignored comparing with the square of cable's length (Li *et al.* 2009), then $T = 4 \frac{m f_n^2 l^2}{n^2}$.

2.2 Damping theory of cable

According to the Rayleigh damping theory (Clough and Penzien 1993), the vibration differential equation of multiple degrees of freedom structure can be expressed

$$[M]\{\ddot{x}(t)\} + [C]\{\dot{x}(t)\} + [K]\{x(t)\} = \{0\} \tag{3}$$

where, $[M]$, $[C]$ and $[K]$ are the mass matrix, damping matrix and stiffness matrix respectively; $[C] = \alpha[M] + \beta[K]$, α, β are the Rayleigh ratios; $\{\ddot{x}(t)\}$, $\{\dot{x}(t)\}$ and $\{x(t)\}$ are the acceleration vector, velocity vector and displacement vector respectively. The Eq. (3) can be rewritten as

$$[A]\{\dot{y}(t)\} + [B]\{y(t)\} = \{0\} \tag{4}$$

where, $\{y(t)\} = \begin{Bmatrix} \{x(t)\} \\ \{\dot{x}(t)\} \end{Bmatrix}$; $[A] = \begin{bmatrix} [C] & [M] \\ [M] & [0] \end{bmatrix}$, $[B] = \begin{bmatrix} [K] & [0] \\ [0] & -[M] \end{bmatrix}$;

Then, the complex eigenvalue equation of state is obtained

$$([A]\lambda + [B])\{\psi\} = \{0\} \tag{5}$$

To solve the Eq. (5), the complex eigenvalues are calculated, which are shown: $\lambda_1, \dots, \lambda_N, \lambda_1^*, \dots, \lambda_N^*$. The relationship among of complex eigenvalues, natural frequency (ω_r) and damping (ξ_r) are as follows

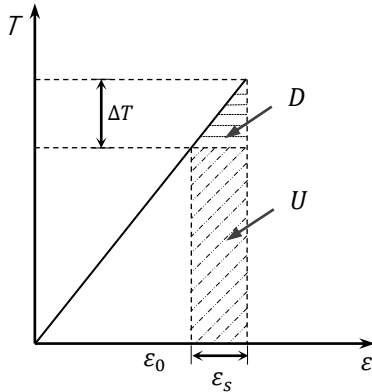


Fig. 2 The potential energy and strain energy of the cable element

$$\begin{cases} \lambda_r = -\xi_r \omega_r + i\omega_r \sqrt{1 - \xi_r^2} \\ \lambda_r^* = -\xi_r \omega_r - i\omega_r \sqrt{1 - \xi_r^2} \end{cases} \quad (6)$$

The natural frequency (ω_r) and damping (ξ_r) are calculated

$$\begin{cases} \omega_r = \sqrt{\lambda_r \lambda_r^*} \\ \xi_r = \frac{\lambda_r + \lambda_r^*}{-2\omega_r} \end{cases} \quad (7)$$

Energy dissipation damping theory is introduced as follows. According to the strain energy dissipated damping theory (Yamaguchi and Adhikari 1995), the modal damping for the i th mode is evaluated as the ratio of the modal dissipated energy per cycle (ΔD_i) to the modal potential energy (U_i)

$$\xi_i = \frac{1}{4\pi} \cdot \frac{\Delta D_i}{U_i} \quad (8)$$

The loss factor η is defined by the ratio of the dynamically dissipated energy (ΔD_i) to the elastic energy stored (D_i) per circle of vibration

$$\eta = \frac{\Delta D_i}{2\pi D_i} \quad (9)$$

As shown in Fig. 2, the modal strain energy (D_i) in the cable due to the dynamic stress from the initial state and the modal potential energy (U_i) due to the initial tension T_0 are as follows

$$\begin{cases} D_i = \int_0^l \frac{EA}{2} \varepsilon_{si}^2 ds \\ U_i = \int_0^l T_0 \varepsilon_{si} ds \end{cases} \quad (10)$$

where, E = the Young's modulus of the cable, A = the area of the cable, and ε_{si} = the modal strain of the element.

2.3 Long-gauge FBG sensors and strain model theory

The technology of distributed strain sensing is greatly required in engineering practices of civil infrastructure

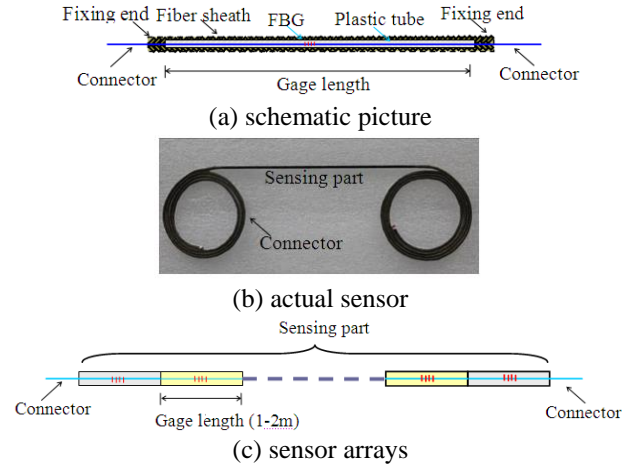


Fig. 3 Packaged LG-FBG sensor

monitoring and maintenance. A long-gauge fiber optic sensor has been developed based on the advantage of the Fiber Bragg Grating (FBG) technology (Chan *et al.* 2006, Li and Wu 2007, Xia *et al.* 2017). By designing the FBG sensor with a long gauge and fixing its two ends (Fig. 3), the in-tube fiber has the same mechanical behavior and hence the strain transferred from the shift of Bragg center wavelength represents the average strain (or say macro-strain) over the sensor gauge length. An improved packaging design has also been proposed to enhance the measuring sensitivity of long-gauge FBG sensors by utilizing two materials with different modulus to package the optic fiber and to impose deformation within the gauge length, largely on the essential sensing part of the FBG (Fig. 3). Due to its long gauge length, the developed LG-FBG strain sensing technique has the merit to measure structural damage (e.g., cracks) in a large area. Furthermore, the long-gauge sensors can be connected in series to make an FBG sensor array (Fig. 3(c)), which is suitable for area macro-strain measuring.

As shown in Fig. 4, a force is input at a node, and structural responses are recorded by both accelerometers and LG-FBG area sensors. Similar to the derivation of the acceleration frequency response function (FRF), the FRF of dynamic macro strain is derived to be (Zhang *et al.* 2016, Zhang *et al.* 2017)

$$\begin{aligned} |{}_r H_{mp}^{\bar{\varepsilon}}(\omega)| &= \frac{\bar{\varepsilon}_m(\omega)}{P_p(\omega)} \\ &= \frac{h_m/L_m \phi_{pr}(\phi_{ir} - \phi_{jr})}{M_r \sqrt{(\omega_r^2 - \omega^2)^2 + (2\xi_r \omega_r \omega)^2}} \end{aligned} \quad (11)$$

where, ω =frequency line, $\bar{\varepsilon}_m$ =macro strain of the element m , P_p =the force at the node p , ${}_r H_{mp}^{\bar{\varepsilon}}$ denotes macro-strain FRF at the mode r , $\omega_r = r^{th}$ the structural frequency, ξ_r = the r^{th} damping ratio, and ϕ =mode shape, h_m =beam cross section height, L_m =element length, M_r =modal mass.

It is seen that the macro strain FRF has a close relationship with the well-known acceleration FRF. Therefore, structural frequencies and damping ratios can also be identified from the poles of the macro-strain FRF.

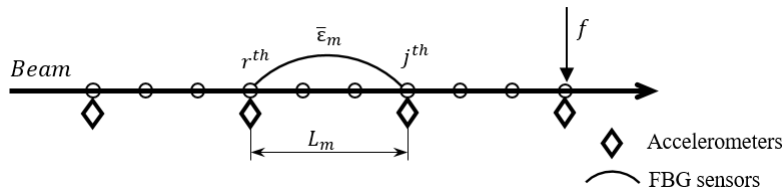


Fig. 4 Strain and acceleration FRFs

Table 1 Material property of experimental cables

Cable	l (m)	α ($^\circ$)	ϕ (mm)	w (g/m)	E (GPa)	σ_u (MPa)
BFRP	6.2	28	13.6	305.1	48.30	1200
BFRP	6.2	28	8.3	113.6	48.30	1200
GFRP	6.2	28	13.6	305.1	51.12	750
GFRP	6.2	28	8.3	113.6	51.52	750

Moreover, the macro-strain FRF more closely resembles a displacement FRF than a velocity or acceleration one, which leads to that the macro-strain FRF provides a more sensitive indicator of structural frequencies at low modes, especially when the resonant frequency of the structure is small.

3. Experimental verifications

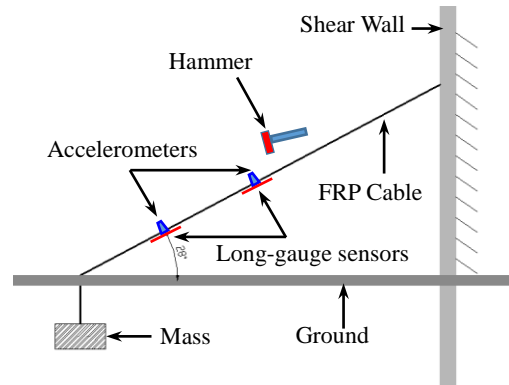
3.1 Design of the vibration test

For the verification of the proposed approach for identifying cable force based on long-gauge strain, the damping characteristics of BFRP and GFRP cables are compared. The vibration test has been conducted. The mechanical properties of FRP cables are listed in the Table 1, and the cables are the products of Green Material Valley Technology Co., Ltd, where l =length of the cable; α =obliquity of the cable; Φ =diameter of the cable; w =weight of the unit length cable; E =Young's modulus of the cable; σ_u =tensile strength of the cable.

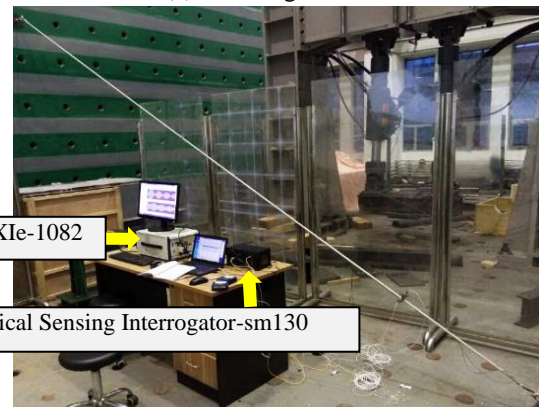
In the experiments, the in-plane and out-plane long-gauge FBG sensors were arranged at the quarter and middle of the cable respectively, and the accelerometers were installed at the same position. The detail testing apparatus are shown in Fig. 5. And in the experiment, the weights were used to increase the cable force.

The maximum stress of the cables in the experiment was 40 MPa, thus the material of the cable was in the elastic stage. The experimental cables are so thin that it is very likely to have some deviations in installing the long-gauge FBG sensors. To avoid this, the static load test was carried out, and then it could be tested that whether the long-gauge FBG sensors were parallel to the cable by using the multi-stage loading strain curves.

After unloading, the multi-stage load was conducted again and the in-plane impact force by hammer was applied on the cable next to the accelerometers respectively in every load case, which was less than 100 N. Besides, the data of acceleration and strain in cable free vibration test was collected by NI Data Acquisition and Optical Sensing Interrogator, as shown in Fig. 5(b). In this experiment, the



(a) Test diagram



(b) The experiments test

Fig. 5 Cables vibration testing

accelerometer is the piezoelectric accelerometer with the type of 393B04, which were bought from PCB Piezotronics, Inc, and the type of the long-gauge FBG sensor was TXD-XF-050X. The sampling rate was set to 1000 Hz.

3.2 Experimental Verifications

3.2.1 Analysis of the cable force

Typical data analysis as follows. Fig. 6(a) shows the measured time history curves of acceleration and strain, which are free-decay responses after impacting test. And the FFT results of the responses are shown in Fig. 6(b). The results show that the identified natural frequencies are almost equal by acceleration and strain.

Fig. 7(a) shows the multi-stage loading strain curves on different position and plane, which reveals that there is some tiny inaccuracy between the different long-gauge FBG sensors, but still basically identical.

According to the calculated $\mu_{max} = l\sqrt{T/EI} = 29.8 < 80$, the flexural stiffness (EI) of the experimental cables

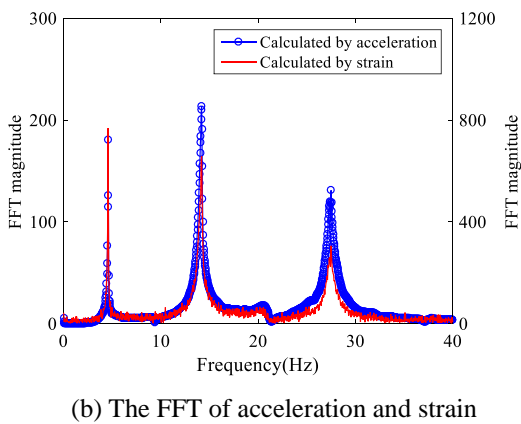
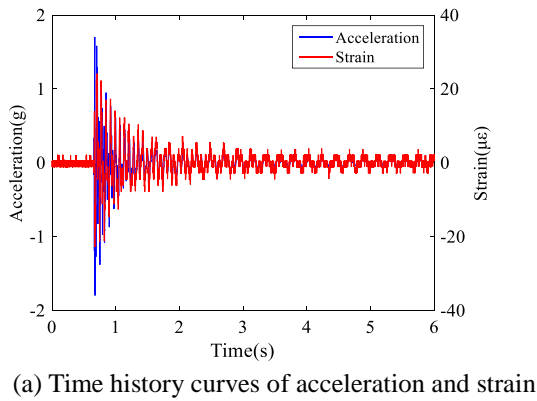


Fig. 6 Time history curves and FFT

Table 2 The measured force of load case for different cables

Cable force (N)	Case 1	Case 2	Case 3	Case 4
Thick BFRP	897.3	1307.3	1720	2183.9
Thick GFRP	943.3	1286.6	1705.3	2242
Thin BFRP	823.7	1192.4	1593.5	2045.6
Thin GFRP	770.8	1114	1560.2	1933.8

have to be considered in calculating cable force by the dynamic test method. The natural frequencies of the cable obtained by the dynamic strain and the acceleration in the vibration test are identical in the same load case, thus the identified cable forces by Eq. (5) are exactly same. Simultaneously, the cable force has been calculated by the static strain.

The cable force by calculating and measuring in different load case are shown in Fig. 7(b). It can be seen that the calculated force by acceleration and dynamic strain are exactly same, and the absolute deviation by different methods is about 50 N. Table 2 lists the measured force under the different load case.

Overall, the long-gauge FBG sensor can obtain the strain time curve with the sample frequency of 1000 Hz. The identified cables force based on the dynamic strain time curve and static strain both have a great precision. So, it is able to check the accuracy of identified cable force based on long-gauge strain by the proposed approach, which offers the doubling guarantees in identifying cable force for engineering. What's more, compared with the traditional approach base on accelerometer, the long-gauge FBG

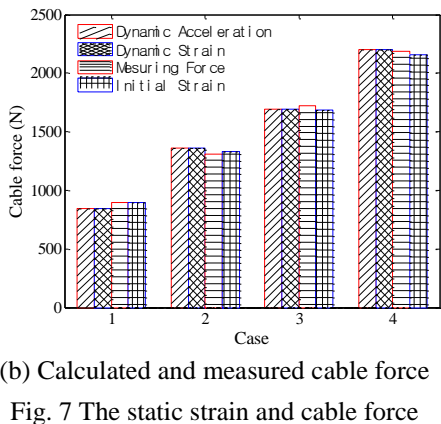
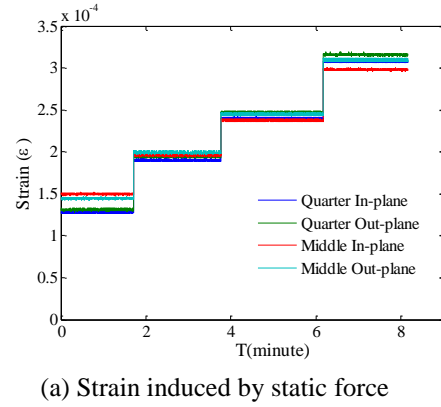


Fig. 7 The static strain and cable force

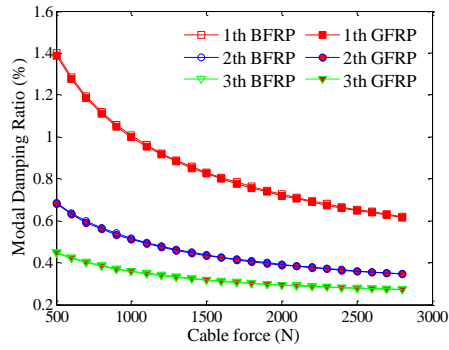
sensors have the advantage of good durability and have an excellent performance in low frequency range. Therefore, the proposed approach for identifying cable force based-on long gauge strain is greatly suitable for long-term monitoring of cable force.

3.2.2 Analysis of the modal damping

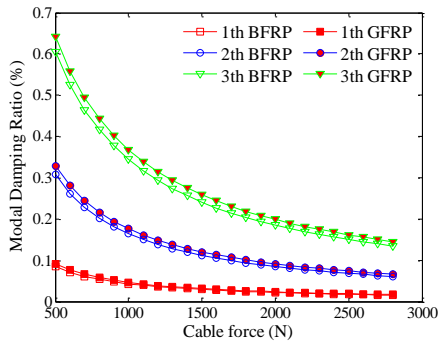
For researching the damping performance of BFRP and GFRP, the calculated distribution of the damping by energy dissipation damping theory and Rayleigh damping theory are discussed first. Assuming that the Rayleigh ratios $\alpha = 0.6$ and $\beta = 1 \times 10^{-5}$, and the energy loss factor of BFRP and GFRP $\eta_B = \eta_G = 0.05$. According to the Eq. (7) and Eqs. (8)-(10), the theoretical damping ratio of thick BFRP and GFRP cables has been calculated.

As shown in Fig. 8, the two damping theories calculation both indicate that the modal damping of cable goes down as the cable force increased, and then gradually becomes gentle. Since the increase of the cable force lead to the cable potential energy and geometry stiffness goes up, which results in the ratio of the strain energy to the potential energy goes down. However, the high order modal damping is smaller than the low order modal damping in Rayleigh damping theory as shown in Fig. 8(a), which is the opposite in energy dissipation damping theory. Besides, Fig. 8(b) illustrates the modal damping ratio of the GFRP cable is little more than the BFRP cable, because of the Elastic modulus of the GFRP cable is slightly larger than BFRP cable.

Based on the half power point method, the first three orders damping ratio has been calculated by the testing



(a) Rayleigh damping theory



(b) Energy dissipation damping theory

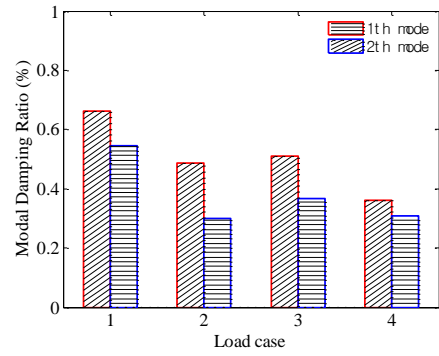
Fig. 8 Distribution of the calculated damping ratio

acceleration data, considering there are some discreteness in the experimental damping ratio, the vibration test has been carried out six times in every load case and selected four close testing data to calculate the modal damping ratio.

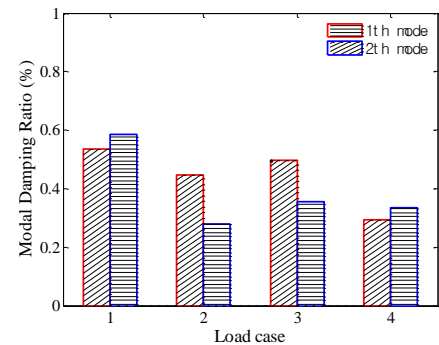
The calculated damping ratios of experimental BFRP and GFRP cables are shown in Fig. 9. The results show that a general trend of the first and second modal damping ratio decreases with the load case increases in the experiment, while the experimental damping results show little discreteness compared with the theoretical distribution of the damping ratio. The second modal damping ratio is smaller than the first modal damping ratio, which coincides with the Rayleigh damping theory. In addition, the modal damping of GFRP cables are generally greater than BFRP cables and thick cables are greater than thin cables. Due to the experimental the first modal damping shows obvious downtrend as the cable force increase, which has been fitted by the energy dissipation damping theory and Rayleigh damping theory.

The fitted curve of modal damping ratio by energy dissipation damping theory shown in Fig. 10. The trend of fitted curves is consistent with the theoretical. The calculated η' is larger than 1 and greater than the loss factor of steel cables and CFRP cables, which η_{CFRP} and η_{steel} are closed to 0.05, which indicates the calculated η' is not the real energy loss factor η and the modal damping of experimental cables are not only the cause for strain energy dissipation, but also the cause of boundary conditions and medium.

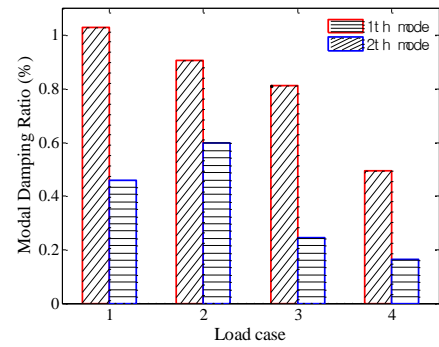
If the Rayleigh ratios are calculated by the experimental natural frequency and modal damping ratio, it would result in error of the calculated Rayleigh ratios α, β due to the



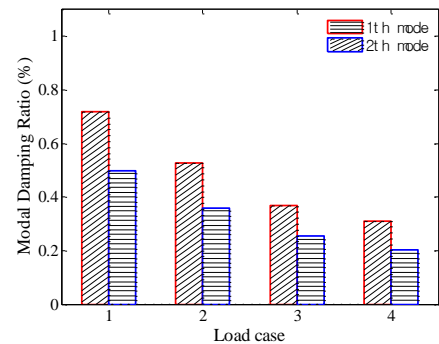
(a) BFRP thick cable



(b) BFRP thin cable



(c) GFRP thick cable



(d) GFRP thin cable

Fig. 9 The testing damping ratio of the cables

testing error, which would cause enormous error in calculating modal damping by calculated Rayleigh ratios α, β . Therefore, the experimental the first modal damping is fitted by Rayleigh damping theory, and the Rayleigh ratios α, β of the cables by fitted are shown in Fig. 11. The distributions of modal damping calculated by Rayleigh

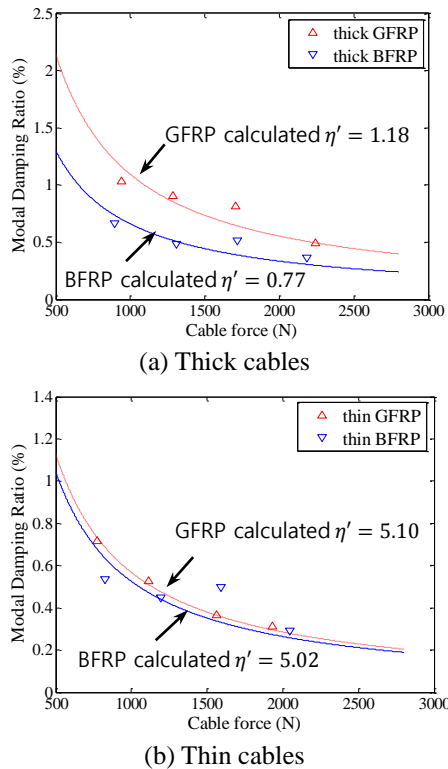


Fig. 10 The fitting modal damping by energy dissipation damping theory

damping theory are closer to the actuals than energy dissipation damping theory, and the damping performance of GFRP cables is better than BFRP cables.

4. Conclusions

According to these experimental results, this study had verified the accuracy of the proposed approach for identifying cable force, and explored the methods to assess the damping performance of BFRP and GFRP. The conclusions are as follows:

The proposed approach based on the combination of both dynamic and static strain has a great precision in cable force identification, and because of long-gauge FBG sensor's good durability and excellent performance in low frequency, it possesses huge potential for long-term monitoring of cable force. The experimental damping of FRP cables decreases with the increase of cable force. The trend of experimental damping changes is similar with the evaluation for modal damping characteristic calculated by Rayleigh damping theory and energy dissipation damping theory. In comparison of the theoretical and testing results, the distribution of modal damping calculated by Rayleigh damping theory is closer to the actuals, and the damping performance of GFRP cables is better than BFRP cables.

Acknowledgments

This work was sponsored by the Chinese National

Science Foundation (Grant No. 51578139). The first author appreciates the support from the Research Innovation Program for College Graduates of Jiangsu Province & the Fundamental Research Funds for the Central Universities (Grant No. KYLX15_0085)

References

- Caetano, E. (2007), *Cable Vibrations in Cable-stayed Bridges*, IABSE, Zurich, Switzerland
- Chan, T.H.T., Yu, L., Ni, Y.Q., Liu, S.Y., Chung, W.H. and Cheng, L.K. (2006), "Fiber bragg grating sensors for structural health monitoring of Tsing Ma Bridge: background and experimental observation", *Eng. Struct.*, **28**(5), 648-584.
- Cheng, L.J. and Karbhari, V.M. (2006), "Design approach for a FRP structural formwork based steel-free modular bridge system", *Struct. Eng. Mech.*, **24**(5), 561-584.
- Clough, R.W. and Penzien, J. (1993), *Dynamics of Structures*, 2nd Edition, McGraw-Hill, New York, NY, USA.
- El Kady, H.M., Arockiasamy, M., Samaan, S. Bahie-Eldeen, Y., Bakhom, M.M., and El Gammal, M.A. (1999), "Damping characteristics of carbon fiber composite cables for application in cable-stayed bridges", *Cable-Stayed Bridges-Past, Present and Future, Proceedings of IABSE Conference*, Malmö, Sweden, October.
- Fujino, Y. and Susumpow, T. (2007), "An experimental study on active control of in-plane cable vibration by axial support motion", *Earthq. Eng. Struct. Dyn.*, **23**(12), 1283-97.
- Irvine, H.M. and Caughey, T.K. (1974), "The linear theory of free vibration of a suspended cable", *Proc. R. Soc. London, Ser. A*, **341**(1626), 299-315.
- Kim, S., Park, J. and Kim, H. (2017), "Damping identification and serviceability assessment of a cable-stayed bridge based on operational monitoring data", *J. Bridge Eng.*, **22**(3), 04016123
- Li, G.Q., Wei, J.B. and Zhang, K.Y. (2009), "Theoretical and experimental study on cable tension estimation by vibration method accounting for rotational end restraints", *J. Build. Struct.*, **30**(5), 220-226.
- Li, H. and Ou, J.P. (2015), "The state of the art in structural health monitoring of cable-stayed bridges", *J. Civil Struct. Hlth. Monit.*, **6**(1), 43-67.
- Li, S.Z. and Wu, Z.S. (2007), "A non-baseline algorithm for damage locating in flexural structures using dynamic distributed macrostrain responses", *Earthq. Eng. Struct. Dyn.*, **36**(9), 1109-1125.
- Nabil, F.G. (2000), "Response of CFRP prestressed concrete bridges under static and repeated loadings", *PCI J.*, **15**(6), 84-102.
- Ren, W.X., Chen, G. and Hu, W.H. (2005a), "Empirical formulas to determine cable tension using fundamental frequency", *Struct. Eng. Mech.*, **20**(3), 363-380.
- Russell, J.C. and Lardner, T.J. (1998), "Experimental determination of frequencies and tension for elastic cables", *J. Eng. Mech.*, **124**(10), 1067-1072.
- Upadhyay, A. and Kalyanaraman, V. (2010), "Optimum design of FRP box-girder bridges", *Struct. Eng. Mech.*, **35**(5), 539-557.
- Wang, X. and Wu, Z.S. (2010), "Modal damping evaluation of hybrid FRP cable with smart dampers for long-span cable-stayed bridges", *Compos. Struct.*, **93**(4), 1231-1238.
- Wu, W.J. and Cai, C.S. (2010), "Cable vibration control with a semiactive MR damper-numerical simulation and experimental verification", *Struct. Eng. Mech.*, **34**(5), 611-623.
- Wu, Z., Wang, X. and Wu, G. (2009), "Basalt FRP composite reinforcements in infrastructure", *Proceedings of the 17th Annual Int. Conf. on Composites/ Nano Engineering (ICCE-17)*,

International Conference on Composites/ Nano Engineering (ICCE), New Orleans

- Xia, Q., Cheng, Y.Y., Zhang, J. and Zhu, F.Q. (2017), "In-service condition assessment of a long-span suspension bridge using temperature-induced strain data", *J. Bridge Eng.*, **22**(3), 04016124
- Xie, X., Zhang, H. and Shen, Y.G. (2008), "Study on characteristics of modal damping of steel and CRP stay cables", *Enr. Mech.*, **25**(3), 151-157.
- Yamaguchi, H. and Adhikari, R. (1995), "Energy-based evaluation of modal damping in structural cables with and without damping treatment", *J. Sound Vib.*, **181**(1), 71-83.
- Yamaguchi, H. and Ito, M. (1997), "Mode-dependence of structural damping in cable-stayed bridges", *J. Wind Eng. Indus. Aerodyn.*, **72**, 289-300.
- Yang, Y.Q., Wang, X. and Wu, Z.S. (2015), "Experimental study of vibration characteristics of FRP cables for long-span cable-stayed bridges", *J. Bridge Eng.*, **20**(4), 04014074.
- Ye, X.W., Dong, C.Z. and Liu, T. (2016), "Force monitoring of steel cables using vision-based sensing technology: methodology and experimental verification", *Smart Struct. Syst.*, **18**(3), 585-599.
- Ye, X.W., Su, Y.H. and Han, J.P. (2014), "Structural health monitoring of civil infrastructure using optical fiber sensing technology: a comprehensive review", *Scientif. World J.*, **2014**, Article ID 652329, 1-11.
- Zhang, J., Cheng, Y., Xia, Q. and Wu, Z. (2016), "Change localization of a steel-stringer bridge through long-gauge strain measurements", *J. Bridge Eng.*, **21**(3), 04015057.
- Zhang, J., Tian, Y.D., Yang, C.Q., Wu, B.T., Wu, Z.S., Wu, G., Zhang, X. and Zhou, L.M. (2017), "Vibration and deformation monitoring of a long-span rigid-frame bridge with distributed long-gauge sensors", **30**(2), B4016014